Check for updates

ADVANCED FUNCTIONAL MATERIALS
www.afm-journal.de

Aligning and Observing the Liquid Crystal Director in 3D Using Small Magnetic Fields and a Wedge-Cell

*Lovish Gulati, Carlos Sánchez-Somolinos, Frank Giesselmann, and Peer Fischer**

The mechanical and optical properties of liquid crystalline materials are largely dependent on the director profile. More complex soft robotic functions and programmed optical properties require spatially varying director profiles, ideally in 3D. However, it is challenging to achieve arbitrary director orientation with most established alignment techniques, as one needs to overcome surface interactions, use high electric or magnetic field strengths and temperatures. Another experimental difficulty is that there is a lack of suitable techniques that can be used to characterize the director in 3D. Here, this study first shows that the addition of 5CB to reactive mesogens permits cross-linked liquid crystalline materials to be fabricated with a spatially varying 3D director profile using weak magnetic fields (0.13 T). This study also shows, how these can be characterized with an optical technique that uses a wedge cell to visualize the programmed 3D director profile. Interestingly, the method also permits the real-time observation of the director. This work shows that it is possible to precisely control the director in 3D with low magnetic fields and that the dynamics can be directly observed, which facilitates potential applications of soft liquid crystalline (LC) gels and potentially also elastomers.

1. Introduction

Cross-linked liquid crystalline polymers (CLCPs) are a class of molecularly-ordered materials that can show a mechanical response to external stimuli such as light, heat, and pH.[1] Depending on the cross-linking density, we distinguish between liquid crystalline networks (LCNs), which are strongly cross-linked systems, and liquid crystal elastomers (LCEs), slightly cross-linked ones typically showing large anisotropic deformation in response to external stimuli such as heat. Addition of low molecular weight LCs to the reactive mesogens results in the formation of swollen CLCPs, commonly referred as liquid crystalline gels (LCGs). The mechanical response of CLCPs is due to the change in the order parameter that creates stresses in the polymer and that lead to the contraction parallel to the director and expansion in the direction perpendicular to it.[2,3] These stimuli-responsive materials can be used for numerous applications, including in soft robotics to realize gripping, crawling, as well as tunable optical devices.[4–11] The mechanical and optical response is thus closely related to the director profile in the cross-linked material.[12] For this, surface alignment,[13–15] nano-/microgroove-based alignment,[16,17] photo-alignment,[18–23] and the application of external fields,[24] were used to fabricate thin CLCPs that can deform in pre-programmed patterns.

Another promising technique to generate a patterned director profile is 4D printing.[25–28] However, especially for extrusion printing, it can be challenging to achieve arbitrary

L. Gulati, P. Fischer
Max Planck Institute for Medical Research
Jahnstr. 29, 69120 Heidelberg, Germany
E-mail: peer.fischer@mr.mpg.de

L. Gulati, P. Fischer
Institute for Molecular Systems Engineering and Advanced Materials
Im Neuenheimer Feld 225, 69120 Heidelberg, Germany

C. Sánchez-Somolinos
Instituto de Nanociencia y Materiales de Aragón (INMA) CSIC-Universidad de Zaragoza Departamento de Física de la Materia Condensada
Zaragoza 50009, Spain

The ORCID identification number(s) for the author(s) of this article can be found under https://doi.org/10.1002/adfm.202413513

© 2024 The Author(s). Advanced Functional Materials published by Wiley-VCH GmbH. This is an open access article under the terms of the Creative Commons Attribution License, which permits use, distribution and reproduction in any medium, provided the original work is properly cited.

DOI: 10.1002/adfm.202413513

C. Sánchez-Somolinos
Centro de Investigación Biomédica en Red de Bioingeniería Biomateriales y Nanomedicina (CIBER-BBN)
Madrid 28029, Spain

F. Giesselmann
Institute of Physical Chemistry
University of Stuttgart
Pfaffenwaldring 55, 70569 Stuttgart, Germany

P. Fischer
Center for Nanomedicine, Institute for Basic Science (IBS)
Seoul 03722, Republic of Korea

P. Fischer
Department of Nano Biomedical Engineering (NanoBME)
Advanced Science Institute
Yonsei University
Seoul 03722, Republic of Korea

alignment, especially out of the plane, as rod-shaped LC molecules tend to align axially due to shear forces and elongational flow.[29] In contrast, the application of external electric and magnetic fields to the LC ink allows, in principle, the orientation in any arbitrary direction prior to polymerization of the LC system. An arrangement of electrodes in a two-photon lithography setup with electric fields of 3×10^5 Vm^{-1}, for instance, permitted the independent alignment of the director in each spatial element.[30,31] For this, rod-shaped LC mesogens were used that possess an anisotropic polarizability to permit their orientation by the applied electric field. Similarly, reactive LC mesogens containing aromatic rings also respond to external magnetic fields. Conjugated aromatics are diamagnetic and hence orient to minimize the magnetic flux passing through them.[32] However, the effect is weak and relatively high magnetic fields of ≈0.3 T have to be applied while also heating the LC ink to near the transition temperature into the isotropic liquid phase, e.g. ≈100 °C.[33] Other approaches used the slow cooling of an LC ink from its isotropic phase to the nematic phase over long periods of time (e.g., tens of minutes) in the presence of relatively high magnetic fields of ≈0.5 T in order to achieve the alignment.[24,34–36]

Despite the relatively low efficiencies of the magnetic alignment, a clear advantage of the field alignment method is that even larger samples on the order of millimeters could be aligned, which is interesting for soft robotic applications, and which is difficult to achieve with surface-based or electric-field-based alignment. A challenge related to electric field alignment are electrohydrodynamic flow effects that are related to the ionic conductivity of the LC and might counteract the E-field alignment.[37]

In any field-driven alignment process it is desirable to reduce the required field strengths and temperatures, while allowing for the 3D orientation of the director. Additionally, a sophisticated director profile – one that varies in position and orientation – can correspondingly give rise to rich mechanical behaviors. It is thus of interest to develop means to permit the observation of the director in 3D, which in turn can assist in the development of suitable alignment techniques. However, it has thus far been challenging to visualize the full orientation of the director using polarization microscopy or X-ray scattering (WAXS / SAXS) measurements.[38,39]

Here, we address these challenges and we report the alignment of the director in any arbitrary orientation using weak magnetic fields. Inclusion of the low molecular weight mesogen 5CB to the reactive mesogens facilitates the director alignment in liquid crystalline gels (LCGs). This has recently also been considered in the work of Wang et al. where they fabricated structures with 2D director alignment at room temperatures.[40] We demonstrated that the director can be aligned in any 3D orientation using low field strengths. We find that three to four times weaker fields are needed for alignment when the mesogen is added in higher concentration compared with magnetic fields that have been reported in other studies.[24,33,34] Furthermore, we report a simple and fast method to characterize the 3D director alignment that also permits the real-time observation of the director in thick samples. The optical characterization technique is based on the splitting of a light beam into an ordinary and an extraordinary ray, as it passes through the birefringent liquid crystalline cell. The ordinary ray has its electric field vector perpendicular to both the director and the propagation direction. The extraordinary ray has an electric field component in the plane of the director and the propagation direction (see also Figure 4a). The splitting is a measure of the director alignment in the cell and permits the visualization of dynamical changes of the director alignment in response to a magnetic field.

2. Results and Discussion

2.1. Magnetic Field Alignment and Ink Formulations

The nematic 5CB, which has a low viscosity, responds well to magnetostatic fields via the anisotropic part of its magnetic susceptibility of $\Delta\chi = 2 \times 10^{-6}$.[41] To minimize the magnetic energy density, the rod-shaped molecules (hence the director) rotate to align with their long axes along the direction of magnetic field.[42,43] Alignment in our setup involves a homogenous field that is provided by two magnets and not a gradient field. **Figure 1a** tries to show this schematically. The alignment of the liquid crystal molecules in our setup is primarily driven by the torque exerted by the magnetic field on the aromatic mesogens having a positive diamagnetic susceptibility, that arises due to zero-net spin and dispersed electron distribution associated with the delocalized charge.[32,36] As expected, the molecular alignment proceeds more easily in less viscous inks.[30] We therefore chose an ink formulation with a low viscosity and to which 5CB can be added. In particular, we used high percentage (49.2%) of the non-reactive LC E7 in our ink formulation, because all the chemicals used for our ink preparation are soluble in E7 and to obtain a nematic phase at room temperature. The chemical structures of the molecules are shown in Figure 1c. We prepared two ink formulations, which we call LCG-ink 1 and LCG-ink 2. The LCG-ink 2 formulation is obtained from LCG-ink 1 after the addition of 20% of 5CB to LCG-ink 1. The viscosity of our LCG-ink 2 formulation is ≈0.13 Pa s, which is about four times higher than that of 5CB. The viscosity data can be found in Figure S1 (Supporting Information) and measurement details are provided in Experimental Section under "Viscosity measurements". The LC alignment in our setup is a function of the response of the liquid crystal molecules to the magnetic field and, since molecules need to re-orient, also a function of the viscosity. The homogenous magnetic field exerts a torque on the aromatic mesogens having a positive diamagnetic susceptibility, which arises due to the delocalized charge of the π-electrons.[32,36] For instance, when comparing the response of 5CB to RM257, the magnetic susceptibility of RM257 (1.87×10^{-6} cm^3 g^{-1})[44] is about ten times larger than that of 5CB (0.17×10^{-6} cm^3g^{-1}),[45] due to the presence of three benzene rings in RM257 compared to 5CB, which has two benzene rings. However, the viscosity of RM257 is much higher (viscosity data for pure RM257 has not been published, but it is highly viscous) and therefore alignment even near its isotropic transition temperature (100 °C) is still relatively slow.[33] However, we also see that our LCG-ink 2 (containing RM257) is more viscous than pure 5CB (see Figure S1, Supporting Information, of Section "Rheological measurements and viscosity"). Even though the magnetic susceptibility is lower, the much lower viscosity of 5CB in the end permits fast alignment with relatively low fields (see also Table S1, Supporting Information, in the Section S2: Alignment response of different inks to the magnetic field

© 2024 The Author(s). Advanced Functional Materials published by Wiley-VCH GmbH

16163028, 2025, 3, Downloaded from https://advanced.onlinelibrary.wiley.com/doi/10.1002/adfm.202413513 by Universidad De Zaragoza, Wiley Online Library on [30/01/2025]. See the Terms and Conditions (https://onlinelibrary.wiley.com/terms-and-conditions) on Wiley Online Library for rules of use; OA articles are governed by the applicable Creative Commons License

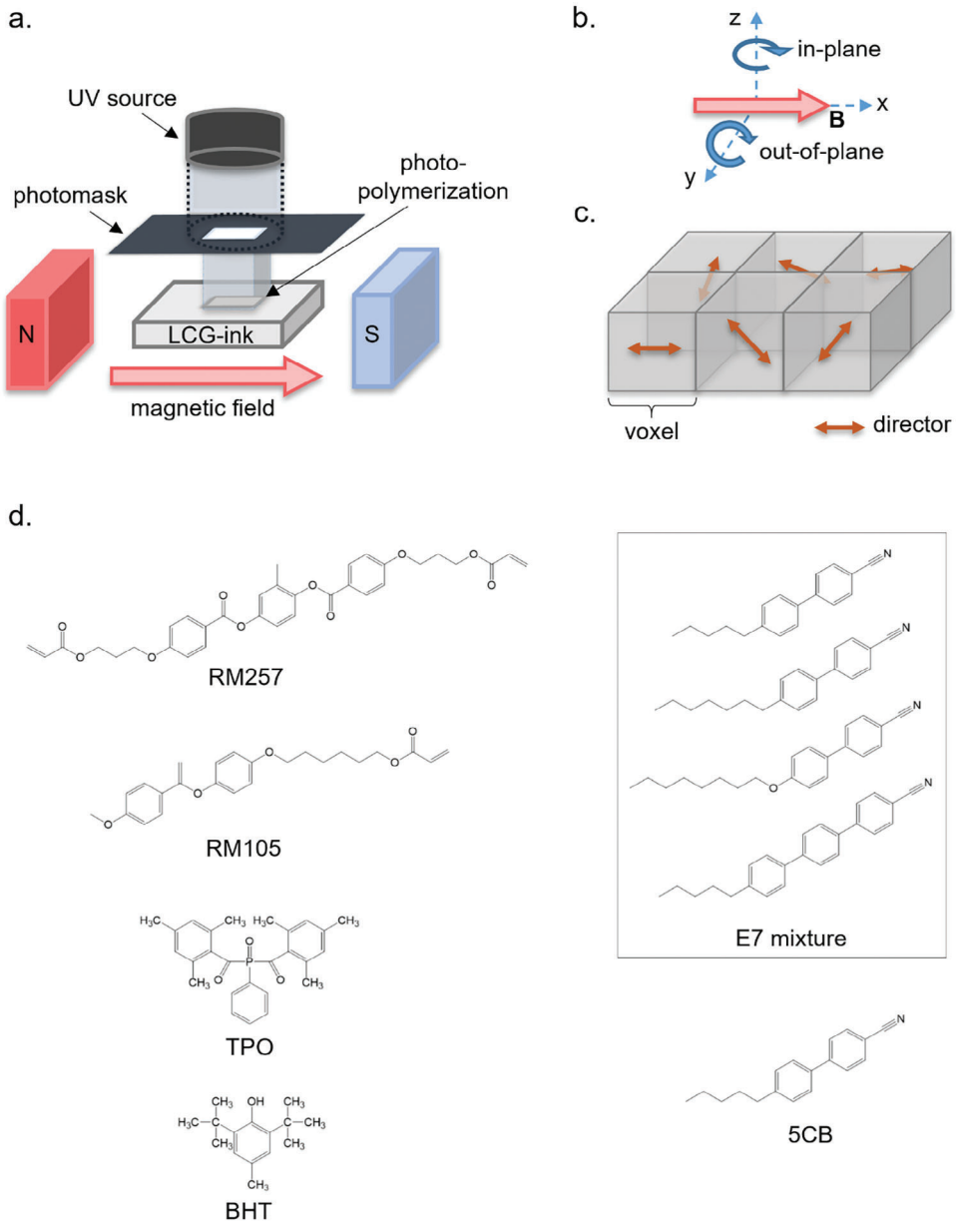

Figure 1. Schematic (not to scale) of the magnetic field alignment of the liquid crystalline gels (LCGs). a) Magnetic field strengths of 0.1 to 0.15 T are provided by two permanent magnets. Gradients are negligible (<3 T m^{-1}). The chamber containing the LCG-ink is aligned with respect to the magnetic field, which sets orientation of the director. The LCG-ink is aligned in 1–2 min. Exposure to UV light for 1–2 min through a photomask induces the polymerization of the exposed region (voxel), while the rest of the sample remains in the liquid state. b) The magnetic field and hence the director can be varied in 3D by orienting the magnets. Both the in-plane and the out-of-plane angles of the director orientation can be fully controlled between 0° and 90°. c) The steps are repeated to form a thin film with programmed 3D director orientation. The arrow denotes the direction of the director alignment for each voxel. d) Molecular structures of the mesogens used to prepare the LCG-ink formulations.

strength). In our ink, 5CB is uniformly distributed throughout the bulk, and when a magnetic field is applied, the 5CB molecules reorient and guide the reorientation of the other liquid crystal mesogens in the process.

First, we examined the alignment of the director as a function of the applied magnetic field strength. The smallest magnetic fields (the so-called threshold field B_0) required to re-align the director was determined by observing the LC cell between crossed polarizers. For these measurements, the LCG-inks were sandwiched in cells with a gap thickness of 250 μm. The relatively large thickness (250 μm) of the cell gap reduces the effect of the surface anchoring on the LC alignment. The LC in the cells initially showed homeotropic alignment in the absence of the magnetic field, and the cell was oriented such that it appeared dark between two crossed polarizers. A magnetic field was then applied in the plane of the cell at 45° to the polarizer and analyzer

© 2024 The Author(s). Advanced Functional Materials published by Wiley-VCH GmbH

16163028, 2025, 3, Downloaded from https://advanced.onlinelibrary.wiley.com/doi/10.1002/adfm.202413513 by Universidad De Zaragoza, Wiley Online Library on [30/01/2025]. See the Terms and Conditions (https://onlinelibrary.wiley.com/terms-and-conditions) on Wiley Online Library for rules of use; OA articles are governed by the applicable Creative Commons License

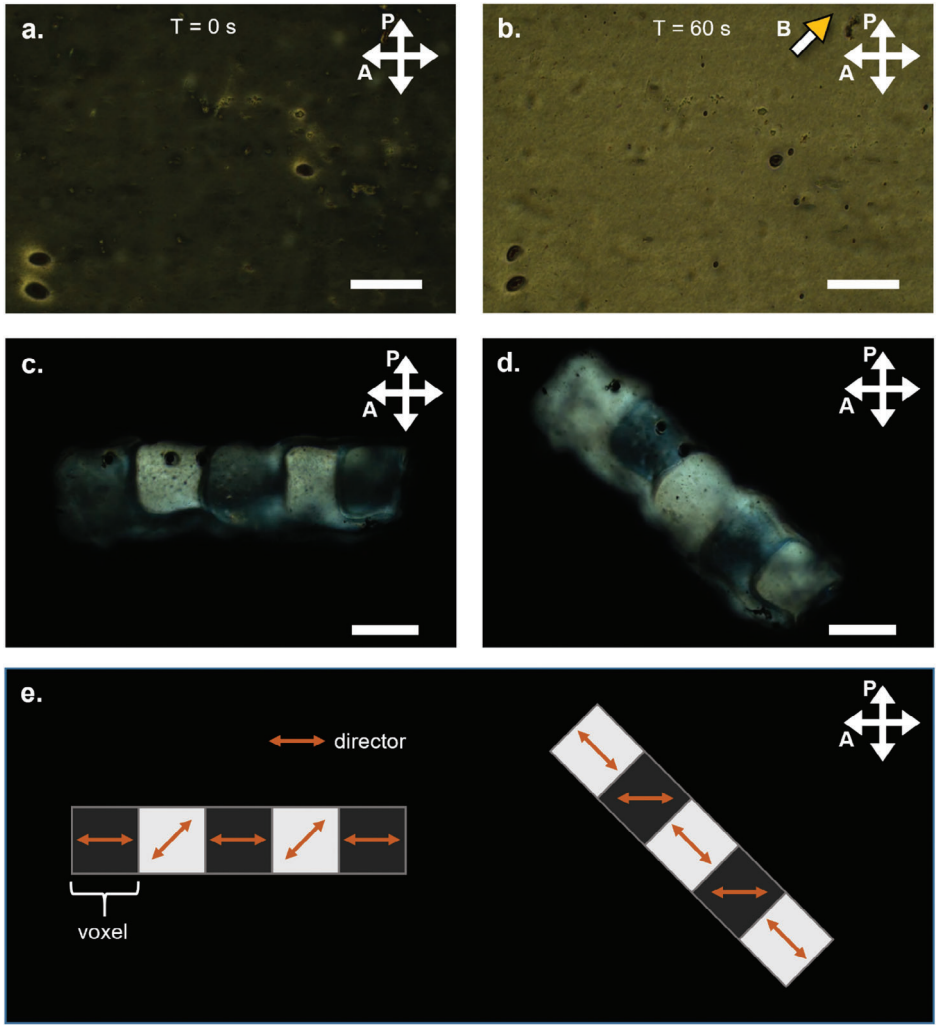

Figure 2. Polarization optical microscopy images of the aligned LC gel and the fabricated LCG ribbon with alternating 2D director orientation. a) Initial alignment of the LCG-ink at time t = 0. The director was aligned parallel to the axis of the polarizers. b) When the magnetic field was applied in the directed depicted by the arrow, the director was oriented at 45 degrees with respect to the polarizers. The alignment was stable after 1 minute and the cell appeared brighter compared to the initial state. c–e) The ribbon was fabricated voxel by voxel with alternate in-plane 2D director orientation by the magnetic field followed by cross-linking. (c) The long axis of the ribbon is parallel to the polarizers which is seen by the alternating brightness of the voxels. (d) The long axis of the ribbon was rotated to 45 degrees which reverses the pattern seen in c). (e) The schematic of the director alignment and corresponding appearance relative to the crossed polarizers. The scale bar is 200 µm.

axes (see **Figure** 2a,b for the magnetic field direction and alignment of LC ink under crossed polarizers). Initially at T = 0s, the alignment was along the polarizer axis. On application of B field at 45° to polarizer axis, as indicated in Figure 2b, the ink appears brighter confirming the orientational response in the direction of the applied field. The threshold field was thus determined visually as the lowest field strength that could re-align the director and cause birefringence changes. Table S1 (Supporting Information) in the under Section "Alignment response of different inks to the magnetic field strength" summarizes the alignment effect of the inks at different magnetic field strengths. We found that LCG-ink 2 formulation containing 5CB of 20% reduces the magnetic field strength required for alignment to that of pure 5CB without compromising the structural integrity of the ink. As shown in Table S1 (Supporting Information), LCG-ink 1 (without 5CB) aligns in a magnetic field of 650 Gauss, whereas pure 5CB and our ink LCG-ink 2 with 20% 5CB align at ≈300 Gauss.[42] Increasing the 5CB concentration beyond 20% would not lead to further reduction in the threshold field strength, but would negatively impact the overall integrity of the structure due to the higher proportion of unpolymerized liquid crystals in the ink. Therefore, 20% 5CB represents an optimal balance between reducing the required magnetic field strength and maintaining structural integrity. It can be concluded that, with the inclusion of mesogens like E7 or 5CB lower magnetic field strengths are needed to re-align the director than the fields used for inks only containing reactive mesogens.[24,33,34]

The magnetic field alignment away from a homeotropic director alignment competes with effects due to surface anchoring, which decreases for molecules farther from the interface. The threshold magnetic field at which re-alignment is observed thus depends on the cell thickness *d*, the anisotropy in the

© 2024 The Author(s). Advanced Functional Materials published by Wiley-VCH GmbH

16163028, 2025, 3, Downloaded from https://advanced.onlinelibrary.wiley.com/doi/10.1002/adfm.202413513 by Universidad De Zaragoza, Wiley Online Library on [30/01/2025]. See the Terms and Conditions (https://onlinelibrary.wiley.com/terms-and-conditions) on Wiley Online Library for rules of use; OA articles are governed by the applicable Creative Commons License

magnetic susceptibility $\Delta\chi$, as well as the elastic constant K of the LC:[32,42,46]

$$B_0 = \frac{\pi}{d}\sqrt{\frac{K\mu_0}{\Delta\chi}} \quad (1)$$

Using the typical values for 5CB, with $K = 10^{-11}$ N, $\Delta\chi = 4\pi 10^{-7}$, as well the experimental conditions of this work where the LC cell has a thickness $d = 250$ µm, we estimate that the threshold field should be $B_0 = 40$ mT (400 Gauss), which is in very good agreement with our experimental observation of the threshold field as listed in the Table S1 of the (Supporting Information). The magnetic coherence length ξ, provides a measure for the distance over which the magnetic field action affects the alignment. The size of coherence length ultimately determines the minimum size of the sample volume in which the director can still be changed by magnetic field. The thickness of this transition layer is given by:[32,46]

$$\xi = \frac{1}{B}\sqrt{\frac{K\mu_0}{\Delta\chi}} \quad (2)$$

Using the material parameters of 5CB, we estimate a magnetic coherence length of $\xi = 32$ µm at $B = 1000$ Gauss. We thus chose a sample thickness >> than the coherence length, i.e., we made LC cells with a gap of 250 µm.

The alignment response of the LC depends, apart from the cell dimensions, on the viscosity and the elastic energy which both decrease at higher temperatures.[47] Previous studies on magnetic field alignment of reactive mesogens thus used high temperatures ≈100 °C (near the isotropic transition temperature T_{NI} of the LCE ink).[24,33,34] The elastic constant K depends on the order parameter S, which decrease at higher temperatures.[43,48]

We observed that the LCG-ink 2 can be aligned in ≈1 min by applying a magnetic field of ≈1300 Gauss at room temperature. This field strength can be obtained in a setup that uses permanent magnets (see Experimental Section: Magnetic field and magnetic field alignment of LCGs). After the alignment, we photopolymerize the ink to obtain soft liquid crystalline gels.[49] Varying the magnetic field direction and subsequent polymerization is used to fabricate LCGs with 2D and 3D director profiles. The LCGs are transparent which facilitates the visualization of the 3D director alignment using polarization optics. In contrast to polarization optical microscopy, which permits the qualitative observation of the director alignment, we describe a characterization technique that uses a wedge cell and permits the precise determination of the director orientation in 3D. This method is based on observing the divergence and polarization of extra-ordinary and ordinary light beams as a function of the director alignment, which defines the optical axis of the system. We first describe the LC alignment by the magnetic field and then provide details of the optical characterization technique.

2.2. Spatial Patterning of a 2D Director Profile

We fabricated liquid crystalline gels with a patterned director profile using LCG-ink 2, which has a lower viscosity and a lower magnetic field threshold for alignment in a LC cell with a gap of 250 µm. The thicker cell, apart from minimizing surface effects, also facilitates the fabrication of self-supporting LCGs. Following magnetic field alignment, the molecular alignment was fixed by exposure to UV light through a photomask. The polymerization is thus restricted to the exposed region (voxel). Upon re-orientation of the magnetic field (defined by the magnets) a new director could be set for each voxel. The unexposed regions of the LC reoriented with the applied field direction, while the exposed region and thus polymerized voxels retained their fixed orientation. By following this procedure iteratively, we fabricated a ribbon whose voxels alternate in their director orientation by 45° with respect to the long ribbon axis. Figure 2c–e shows the polarization optical microscopy (POM) images of the ribbon with alternate director orientation of 0° and 45°.

The experimental observations of Figure 2 thus far demonstrate the formation of patterns in LCGs where the director can be oriented with smaller magnetic fields. The effect of the field on the director alignment in the plane of the LCGs is readily observed using crossed polarizers. In the next step, thermal response of the uniaxially aligned liquid crystal network was tested to understand the mechanical deformations of these structures to external stimuli.

2.3. Thermal Response of Uniaxially Aligned Liquid Crystal Networks (LCNs)

After cross-linking the LC gel, the un-polymerized part of the LCG was washed out. After drying, the liquid crystalline networks were heated and observed in a polarization microscope. **Figure** 3a,b shows that the director alignment is retained in the LC network when viewed under crossed polarizers. Figure 3c,d shows the response of the LCN at high temperatures resulted in the anisotropic shape change. In this experiment, we have repeated the actuation and Figure 3 shows the response for the 2nd cycle. We observed that this structure shows a contraction of 20% along the director and it expanded in-plane by 15% perpendicular to the director alignment. The deformation reached a maximum at 200 °C. On cooling, this network relaxed back to its original shape. These deformations can be understood on the basis of changes of molecular alignment.

The observed thermal response validates the effective mechanical performance of LCNs created with LCG-ink 2, which has been aligned with low magnetic fields during fabrication.

2.4. Characterization of the Director in 3D

2.4.1. Wedge Cell Technique

The polarization optical microscope (POM) is useful to determine the director or its perpendicular orientation in a plane orthogonal to the imaging direction. It follows that a director that is oriented along all three spatial directions will thus be observed as a projection in this plane. It is thus not straightforward to measure the 3D molecular orientation in a birefringent sample. POM can thus not be used to directly determine the out-of-plane angle of the director. The LC-PolScope is one instrument which can be

© 2024 The Author(s). Advanced Functional Materials published by Wiley-VCH GmbH

16163028, 2025, 3, Downloaded from https://advanced.onlinelibrary.wiley.com/doi/10.1002/adfm.202413513 by Universidad De Zaragoza, Wiley Online Library on [30/01/2025]. See the Terms and Conditions (https://onlinelibrary.wiley.com/terms-and-conditions) on Wiley Online Library for rules of use; OA articles are governed by the applicable Creative Commons License

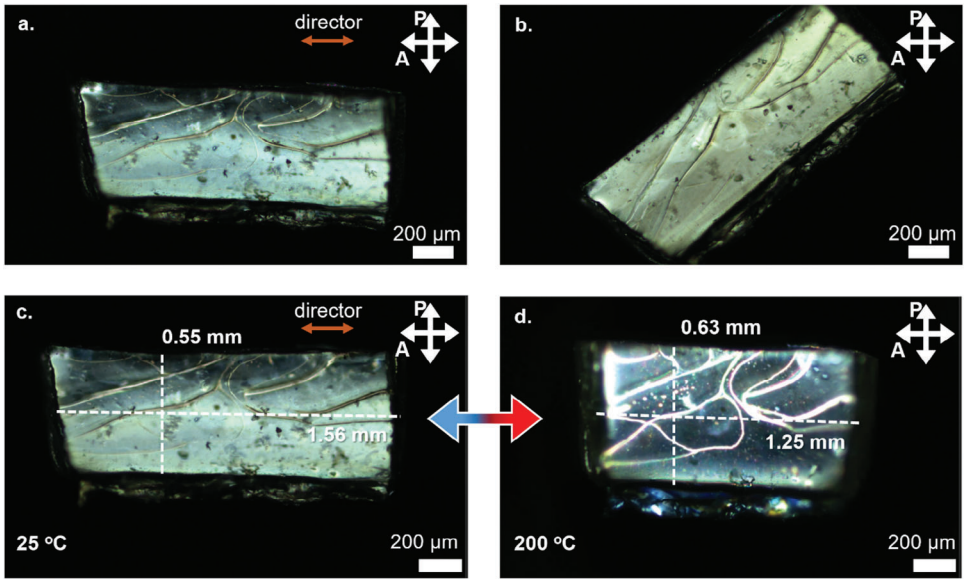

Figure 3. Liquid crystalline network alignment and thermal contraction observed under crossed polarizers. The developed liquid crystalline network is manually rotated. a) The LCN with director orientation along the direction of the analyzer (A) transmits less light compared to the network b) that is rotated by 45° with respect to the axis of the polarizer (P) which appears brighter. The defects are cracks that appeared after the drying step. c,d) Thermal response. When the temperature was raised to 200 °C, the length of the structure contracts by ≈20% along the long axis and expands by ≈15% along the short axis, after the second cycle in the thermal actuation. as seen in d).

used to measure the 3D orientation, but it requires a special setup that uses sequential illumination with circular- and elliptically-polarized light of different axis directions to image the projection of the director (or optical axis) and the optical path difference in 2D at the same time. The off-plane angle can then be calculated from the latter.[50] Therefore, a simpler characterization technique is needed to visualize the director orientation. Also, more complex director profiles of liquid crystalline materials are of interest when realizing actuators and sensors, which necessitates a method that can be used to examine the orientation in all three spatial directions – ideally in real-time. This can be achieved with an optical characterization technique that is based on the splitting of the light beam when it passes through a birefringent medium.

In the LC sample with nematic order, the optical axis is along the same direction as the aligned director. When the light beam, conveniently provided by a laser, enters a birefringent material, then it splits into two components, termed the ordinary ray (O-ray) and the extraordinary ray (E-ray), the polarization planes of which are perpendicular to each other. For the case of normal incidence of the beam to the optic axis, the O-ray has its electric polarization vector orthogonal to the optic axis (direction of the director) and the E-ray has the electric field vector pointing along the optic axis (direction of the director). The E-ray and the O-ray experience different refractive indices which can be represented as n_o and n_e respectively. But for the beam propagating in the birefringent medium at an angle θ to the optic axis, the angular dependence on n_o and n_e gives rise to an effective index of refraction for the extraordinary component of the light ray:[51–53]

$$n_{\text{eff}}^2(\theta) = \frac{n_e^2\, n_o^2}{n_o^2 \sin^2\theta + n_e^2 \cos^2\theta} \tag{3}$$

The propagation direction of the E-ray is determined using n_{eff} in conjunction with Snell's law and the wedge angle. For any other arbitrary director alignment (optic axis), the E-ray experiences an effective refractive index n_{eff} so that $n_e \geq n_{\text{eff}} \geq n_o$. Due to different refractive indices, when a light beam enters in a birefringent medium at an angle θ to the optic axis, the E-ray and O-ray components propagate in different directions. The effective birefringence gives rise to the separation between these rays and in our analysis. We have used this separation as a measure to determine the out-of-plane director alignment from the cell walls.

In the case of a parallel plate cell filled with the birefringent liquid crystal and a light beam that is incident normal to the cell, the ordinary and extraordinary component propagate at different angles inside the medium. The O-ray travels along the normal into the cell medium. The E-ray moves in a direction of ≈0° to 6° relative to the direction of optic axis.[52] When both rays exit the cell, they do so with slight displacement. Since they then travel parallel to each other the displacement stays constant. The displacement is small and hard to observe for thin samples. The beam separation varies between 0 and ≈25 µm, while the beam itself had a diameter of 500 µm. Therefore, a wedge cell (cf. **Figure 4**) was used as here the O- and the E-ray continue to diverge after they exit the cell. A wedge cell has been used previously for the measurement of refractive indices of nematic liquid crystals.[46,54] Here, we show that it is also useful to determine the director orientation in 3D.

In the case of a liquid crystalline medium in a wedge cell, polarized light entering at the optical surface with normal incidence thus separates depending on the state of polarization of the light beam and depending on the orientation of the director.[51,52,55] As shown in the Figure 4, the LC cell has its director perpendicular to the propagation direction of the beam. Assuming that the

© 2024 The Author(s). Advanced Functional Materials published by Wiley-VCH GmbH

16163028, 2025, 3, Downloaded from https://advanced.onlinelibrary.wiley.com/doi/10.1002/adfm.202413513 by Universidad De Zaragoza, Wiley Online Library on [30/01/2025]. See the Terms and Conditions (https://onlinelibrary.wiley.com/terms-and-conditions) on Wiley Online Library for rules of use; OA articles are governed by the applicable Creative Commons License

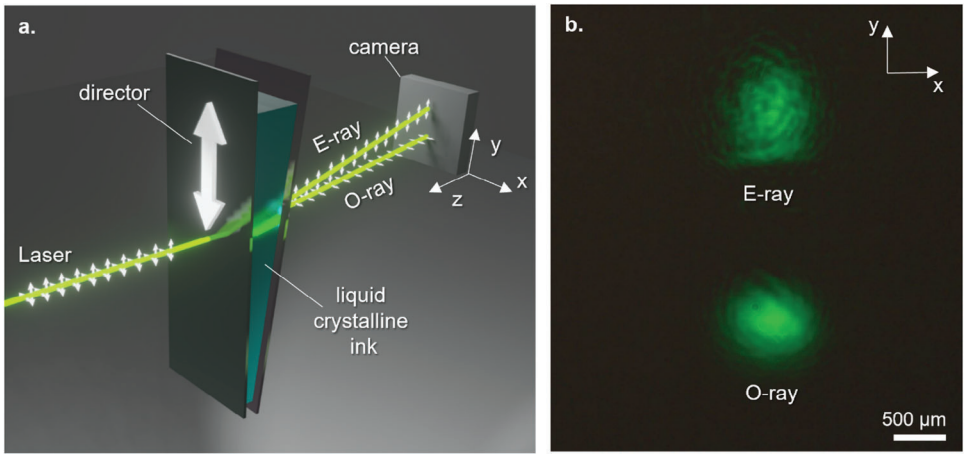

Figure 4. Wedge cell used to determine the 3D director alignment. a) The unpolarized laser beam is incident normal to the first face of the wedge cell. The white double-arrows indicate the light ray's polarization and thus the corresponding plane of the electric field. The transmitted light from the wedge cell splits into two components: the ordinary (O) and the extraordinary (E)-rays. The E-ray is polarized in the direction parallel to the plane formed by the director and the propagation direction. The O-ray has its polarization direction perpendicular to the director. A possible director orientation is depicted by the white double-headed arrow. The refraction of the beams depends on the wedge angle of the cell and the orientation of the director. b) The beam spots of the E-ray and O-ray are detected by a camera at distance (here 8.3 cm) from the angled cell window.

director is uniformly aligned throughout the whole thickness of the cell. At the interface of isotropic and birefringent medium, due to the difference in the refractive indices for the O- and the E-ray, the beams will split in different directions by following Snell's law and the wedge angle.[56]

We prepared the wedge cell as described in the Experimental Section under "Preparing the wedge cell". A 532 nm laser (0.4 µW) was used for the optical measurements on the birefringent LC sample. The extraordinary and ordinary light beams were imaged by a CCD camera mounted at 8.3 cm from the exiting window of the wedge cell. As seen in the schematic of Figure 4a (also Video S1, Supporting Information), the laser beam with normal incidence at the air-glass-LC interface transmits into and propagates through the LC medium as one beam. However, at the other side of the cell, the angle of incidence at this second LC-glass-air interface is equal to the wedge angle. Because of the different refractive indices for the E-ray and O-ray in the birefringent medium, these rays exit the cell at different angles. This difference in the angles of refraction leads to a divergence which leads to a separation of the O-ray and E-ray at the camera. The splitting is thus a function of the birefringence and the orientation of the director.

To estimate the divergence angle between the O- and E-rays, the refraction angle θ_e of the E-wave at interface 1 needs to be determined. For a fixed incidence angle θ_i the refraction angle θ_e depends on the direction cosines of the optic axis as derived in the Supplementary Information "Section S3 (Supporting Information): Refraction at the interface of a birefringent LC medium". The relation [Equation S10, see Supporting Information] is valid for any arbitrary 3D orientation of the optic axis in a birefringent medium. For the experiments we conducted this further simplifies, as the incidence angle $\theta_i = 0°$ such that $\theta_o = \theta_e = 0°$, as can be seen in **Figure 5a**. The splitting between the O- and E-wave arises at interface 2 where the incidence angle is equal to the wedge angle δ. The divergence angle α is obtained using Snell's law and depends on the effective refractive index of the E-wave. The

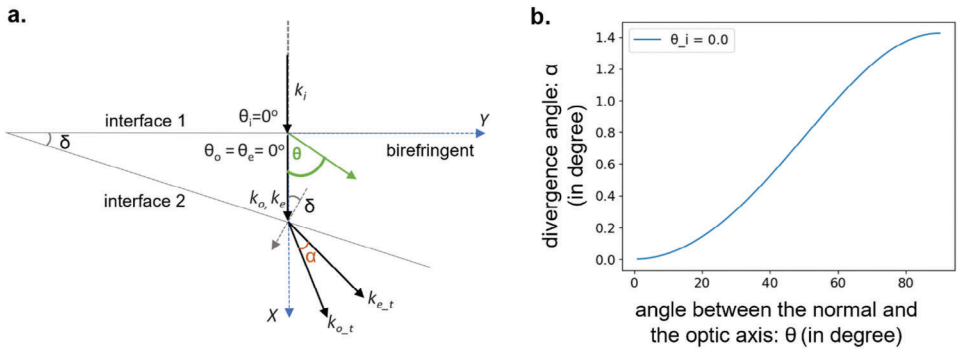

Figure 5. a) Schematic showing a beam with normal incidence onto the wedge cell leading to a divergence between the E-ray and the O-ray. Both the E- and O-wave propagate normal to the interface 1 inside the birefringent medium. For an arbitrary orientation of the optic axis, the angle with respect to the normal of interface 1 (θ, as depicted in the schematic) is considered. b) Plot of the divergence angle as a function of the out-of-plane angle θ of the optic axis, assuming a wedge angle $\delta = 7°$.

© 2024 The Author(s). Advanced Functional Materials published by Wiley-VCH GmbH

16163028, 2025, 3, Downloaded from https://advanced.onlinelibrary.wiley.com/doi/10.1002/adfm.202413513 by Universidad De Zaragoza, Wiley Online Library on [30/01/2025]. See the Terms and Conditions (https://onlinelibrary.wiley.com/terms-and-conditions) on Wiley Online Library for rules of use; OA articles are governed by the applicable Creative Commons License

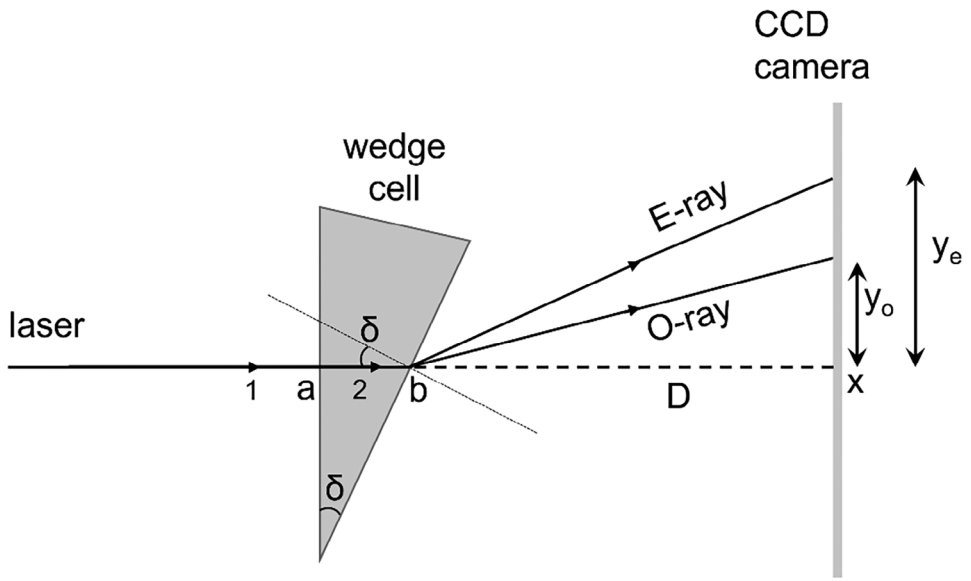

Figure 6. Schematic showing the refraction of the laser beam while passing through the wedge cell. The laser beam enters the cell at point a and propagates through the birefringent ink. The E-ray and O-ray refract with different angles of refraction after exiting the cell at point b. The wedge angle δ enters Snell's law. The beams diverge and are imaged at the distances y_e and y_o from the reference point x.

effective refractive index depends on direction of the optic axis θ. The plot in Figure 5b shows the divergence for a wedge angle $\delta = 7°$ and typical refractive indices, where $n_o = 1.5$ and $n_e = 1.7$. It is seen that the divergence angle increases as the angle of the optic axis increases with respect to the normal of interface 1. Hence, by measuring the divergence angle, one can estimate the orientation of optic axis and thus the orientation of the LC director.

Figure 6 shows a schematic (not to scale) of the wedge cell characterization experiment to analyze out-of-plane director orientation. The entrance face was oriented such that the laser beam entered the wedge cell at normal incidence. The distance "D" of the exit window to the camera was measured and the center position of the observed beam spots was measured on the screen ("y_o" and "y_e") relative to the point x, as depicted in the schematic, where the light beam would have entered the camera, if there was no wedge cell in the path of the laser.

2.4.2. Analysis of In-Plane Director Orientation

A polarization analysis can be used to determine the orientation of the director. If the incident light is linearly polarized, one can determine the in-plane director projection to the cell substrates. By rotating the polarization direction of the incident light, it is possible to change the relative intensities of the E- and the O-ray spots as imaged by the CCD camera. These two beams were separated by distance d as seen in the panels of **Figure 7**. Video S2 (Supporting Information) shows that when the polarization direction aligns with the plane defined by the director and propagation direction, only the E-ray passes through the cell. When the polarization plane of the incident light is rotated by an additional 90°, then only O-ray passes through the cell, as expected. This was confirmed using an analyzer in the beam path after the cell. When the analyzer is introduced with its optics axis in the plane formed by the director and the propagation direction, then the O-ray is blocked. Only one "spot" is then seen on the camera, corresponding to the extraordinary component of the light. Similarly, when the analyzer has its optic axis perpendicular to the director, then the E-ray is blocked. Therefore, knowing the incident polarization direction of the incident beam, one can measure the in-plane director orientation of the 3D director profile.

2.4.3. Analysis of Out-Of-Plane Director Orientation

The separation between these two rays depends on various factors, such as wedge angle, angle of incidence of the laser, as well as the orientation of the director. Since the first two are experimentally known, the wedge cell technique can be used to determine the 3D director alignment.

Figure 7 shows the observed separation for different out-of-plane angles, θ. The separation between the E-ray and the O-ray was large when the magnetic field (and hence the director) was oriented in the plane of the cell ($\theta = 90°$). This separation decreased, when the magnetic field (director) pointed 45° out of plane. Video S3 (Supporting Information) shows the dynamics of splitting when the director alignment was changed from 0° to 45° to 0° out-of-plane angle during the observation. The laser spot on the camera is seen to split. The separation between the two components thus provides a real-time measure of the birefringence and hence the director alignment as a function of the aligning magnetic field.

2.4.4. Splitting Observations for Different 3D Director Orientations

The wedge cell technique was used to determine the orientation of a director that possesses an arbitrary direction, i.e., described

© 2024 The Author(s). Advanced Functional Materials published by Wiley-VCH GmbH

16163028, 2025, 3, Downloaded from https://advanced.onlinelibrary.wiley.com/doi/10.1002/adfm.202413513 by Universidad De Zaragoza, Wiley Online Library on [30/01/2025]. See the Terms and Conditions (https://onlinelibrary.wiley.com/terms-and-conditions) on Wiley Online Library for rules of use; OA articles are governed by the applicable Creative Commons License

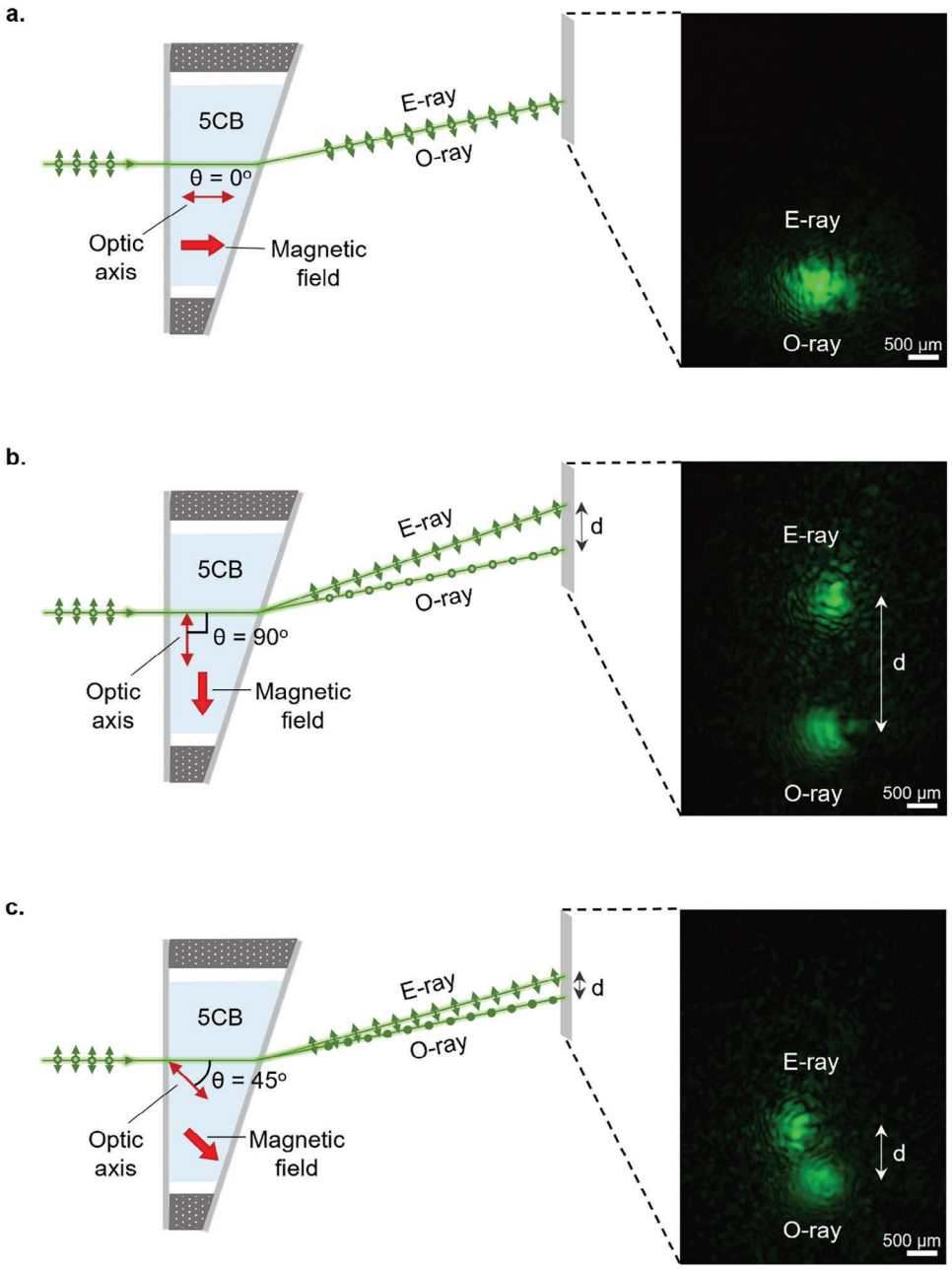

Figure 7. The separation distance between E-ray and O-ray on the imaging screen is a function of the out-of-plane director alignment. Three different director orientations with angle θ measured from the direction of propagation of the laser are depicted. The optical axis of the birefringent nematic LC is the same as the director alignment direction. a) When $\theta = 0°$, there will be no birefringence encountered by the laser beam and the E-ray and O-ray do not split and are coincident at the same spot on the camera. b) When $\theta = 90°$, the maximum birefringence of the LC medium is sensed by the laser beam, which results in a maximal divergence and hence a maximal separation distance d on the camera. c) In this case, $\theta = 45°$, the effective refractive index n_{eff} of the E-ray component decreases, which reduces the effective birefringence for the two orthogonal polarization directions of the incident beam. Therefore, the splitting between the E-ray and O-ray increases as the angle θ increases from 0° to 45° and then to 90°.

by two Euler angles. For this, liquid crystalline ink was aligned in seven different 3D orientations in wedge cells and then cross-linked prior to the optical characterization. **Figure 8** shows the schematic depicting the director alignment in each cell. To obtain the different director orientations, the magnetic field was first rotated in plane to the angles φ:0°, 45° & 90° (see Figure 8), as well as along the out-of-plane angles θ: 0°, 45° & 90°. The angle φ was measured by rotating the polarization of the incident light using a half-wave plate. The polarization angle, at which the ordinary ray component completely vanished, corresponds to the angle φ. To determine the angle θ, the splitting between the E- and the O-ray was measured (see Section "S4 (Supporting Information): Protocol to determine the 3D orientation of the LC director in a wedge cell"). As expected, the separation was largest for the

© 2024 The Author(s). Advanced Functional Materials published by Wiley-VCH GmbH

16163028, 2025, 3, Downloaded from https://advanced.onlinelibrary.wiley.com/doi/10.1002/adfm.202413513 by Universidad De Zaragoza, Wiley Online Library on [30/01/2025]. See the Terms and Conditions (https://onlinelibrary.wiley.com/terms-and-conditions) on Wiley Online Library for rules of use; OA articles are governed by the applicable Creative Commons License

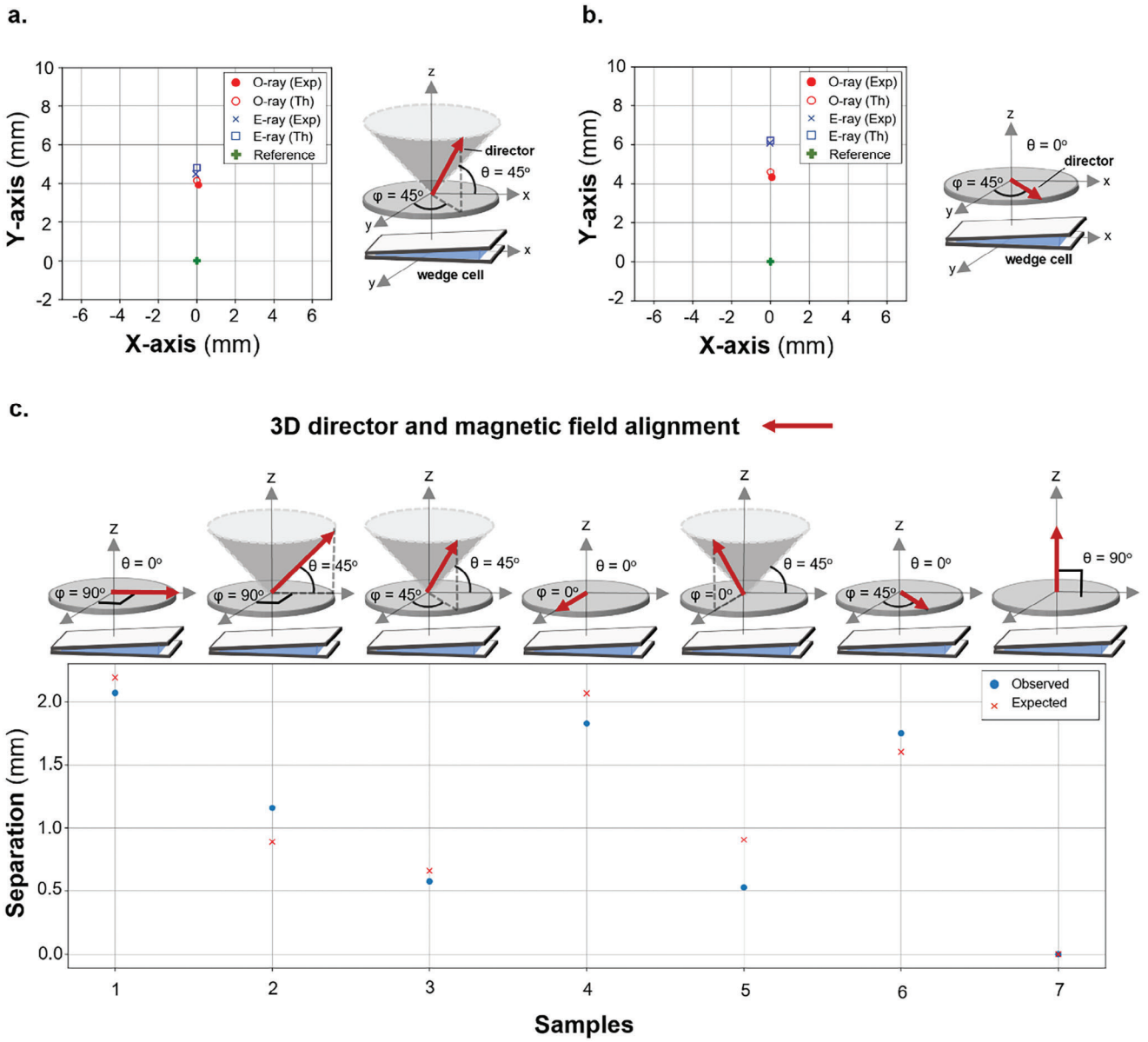

Figure 8. Observed splittings between the E- and the O-ray in a wedge cell and comparison with theoretical estimates. The angles θ and φ are varied using a polarizer. This provides an estimation of the reliability of the characterization technique. The director alignment, magnetic field direction, and optic axis all are depicted by the same red arrow. a–c) Theoretical calculations demonstrate that the separation distance as a function of director alignment matches well with the experimental data points. (a) $\theta = 45°$ and $\varphi = 45°$ leads to a smaller separation distance, which is even more pronounced in the configuration (b) with $\theta = 90°$ and $\varphi = 45°$. These results show the dependence of the observed splitting with out-of-plane angle θ. (c) The splitting between the two orthogonal perpendicular polarization components depends mainly on the angle θ, for any in-plane angle φ. The difference in the splitting between the samples having same off-plane angle θ, is due to the small difference in the wedge angle of the corresponding wedge cell. When $\theta = 90°$ (samples 1, 4 and 6), the observed separation distance is larger, because of the high effective refractive index n_{eff} for E-ray. For samples 2,3 and 5: $\theta = 45°$ resulting in a lower n_{eff}, and hence a smaller separation distance. The separation distance as a function of θ can be related to the director alignment direction (optic axis).

director with $\theta = 0°$ for all three φ angles. When the director was oriented with $\theta = 45°$ for all φ angles, the separation decreased. The separation distance could be compared to the theoretical predictions and both match well, as can be seen in Figure 8.

Furthermore, the dynamics of the magnetic field alignment is visualized for the application of a magnetic field to 5CB in the wedge cell (see also Video S3, Supporting Information). The real-time measurement also provides information on the time required to orient the LC, here with a magnetic field of 1000 G. Observation of the alignment dynamics can be used to optimize inks, cells, and fields to obtain the correct 3D alignment required by a particular application.

Hence, low magnetic fields can enable the fabrication of 3D aligned films that can potentially exhibit complex actuation

© 2024 The Author(s). Advanced Functional Materials published by Wiley-VCH GmbH

16163028, 2025, 3, Downloaded from https://advanced.onlinelibrary.wiley.com/doi/10.1002/adfm.202413513 by Universidad De Zaragoza, Wiley Online Library on [30/01/2025]. See the Terms and Conditions (https://onlinelibrary.wiley.com/terms-and-conditions) on Wiley Online Library for rules of use; OA articles are governed by the applicable Creative Commons License

behaviors. Our fabricated 3D aligned films were sticky and too soft to handle post fabrication. Hence, we did not pursue thermal actuation in our experiments further. However, the literature indicates that one can expect not only in-plane contraction and expansion, but rather a complex response, where the deformation angle depends on the out-of-plane director alignment.[34]

In our wedge cell characterization experiments (see Figure 8), a splitting angle between the E-ray and O-ray in the range of 0° to 1.5° was observed depending on the out-of-plane orientation angle theta θ (varied from 0° to 90°) for a wedge angle δ of ≈7°. The splitting is readily observed by placing the camera detector at few centimeters away from the wedge cell. This characterization technique can also potentially provide dynamical information and be used to determine the parameters that determine the LC director alignment. For weak magnetic fields, small divergence angles and weak effects one can potentially amplify the splitting between the E-ray and O-ray using a weak value amplification scheme. Weak value amplification uses a carefully chosen post-selection for the final polarization state of a light beam and has been successfully applied to observe nanorad divergence angles in optically active systems.[57,58] This will further enhance the sensitivity of the present method and thus permit samples with very small birefringence (compared to 5CB) to be characterized.

The method presented herein also has some limitations, but these are general to any voxelated LC alignment procedure. Surface anchoring effects influence the alignment at the boundary of each voxel. Dramatic changes in alignment from voxel to voxel therefore incur an energy cost. In addition, the minimum voxel size for 3D alignment is constrained by the magnetic coherence length (here $\xi = 32$ µm). In voxels where the characteristic dimensions (e.g., 250 µm for the 2D ribbon structure shown in Figure 2c,d) are much larger than ξ, the influence of surface anchoring effects from adjacent voxels diminishes exponentially.[32] As a result, the alignment within each voxel is primarily governed by the applied magnetic field, rather than by interactions with neighboring voxels. Specific to the optical characterization method we describe is the use of a wedge cell. While it offers real-time visualization of the director, and thus also an approach to quantify surface effects, the use of a wedge cell is not as practical as a parallel cell. Therefore, one can first use a wedge cell to optimize parameters such as ink composition, field strengths, surface coatings, and alignment response times, and after the optimization, one can switch to a desired cell to prepare aligned LC structures.

The magnetic alignment method offers considerably more versatility compared to other alignment techniques, allowing for precise 3D control of the director orientation, which is crucial for encoding mechanical responses in LCE actuators. While the current film's softness may have limitations in robotic actuation, the alignment method and the precise characterization scheme should be useful for optimizing crucial process parameters. The optical characterization method is also general and allows for the real-time visualization of 3D director alignment of any LC, which is of interest in other fields and different surface alignment techniques. The method can therefore be used to verify and diagnose the quality, limitations, and uniformity of director alignment procedures. Once these aspects are satisfactorily addressed, the same process can be applied to fabricate structures with more complex designs and director profiles.

We have also demonstrated an example to fabricate small optical elements, such as Wollaston Prism (see Supplementary Information "Section S5 (Supporting Information): Fabrication of Wollaston Prism using liquid crystal gel ink"). The goal is to demonstrate the potential applications of this method to fabricate complex optical elements that are not easily realized with other techniques.

3. Conclusion

We have first demonstrated that the addition of 5CB lowers the threshold field to align liquid crystal inks with a magnetic field leading to cross-linked LC materials. Our LCG-ink containing the mesogen E7 and 5CB could thus be aligned with field strengths of ≈0.13 T at room temperature. We could show a way to fabricate liquid crystalline gels with a spatially varying director profile. We also oriented the director in arbitrary directions in 3D and developed a method to optically determine the orientation of the director. The optical characterization technique offers an effective way to visually determine the out-of-plane angle of the director profile that cannot be determined using polarization optical microscopy alone. The technique is based on the splitting of a light beam into two orthogonal polarization states when it refracts through a wedge cell containing the nematic LC. Observing the splitting thus provides a real-time measure of the birefringence and hence the director alignment in the LC. The dynamical change of the director in response to changes in the magnetic field direction could thus be observed. The method is expected to facilitate the development of LC systems with complex director profiles. A ribbon with 2D director patterns was shown, as well as a patterned LC network (LCNs) that showed mechanical deformation upon heating. We believe that our work aids the fabrication of LC systems with complex director profiles by demonstrating that the necessary field strengths can be lowered and by providing a method to observe the director alignment in 3D, especially in real-time. Further work should focus on additional ink formulations, where there is a more complete cross-linking, as the presence of unreactive mesogens causes changes in the structures' dimensions. Preferable are inks that can be aligned at room temperature. Additionally, synthesizing magnetic particles that can locally interact with the director and influence global director alignment could be beneficial, however, the challenge in this case is to avoid aggregates and defects. Liquid crystalline polymers with spatially varying 3D director profile can be used as soft responsive materials. The higher degree of control in the director programming will lead to stimuli-responsive materials that are hard to realize with other alignment techniques.

4. Experimental Section

Chemicals and Inks: The molecular structures of the chemicals used are depicted in Figure 1d. The reactive mesogens 4-Methoxybenzoic acid 4-(6-acryloyloxy-hexyloxy)phenyl ester (RM 105) (**1**), 4-bis[4-(3-acryloyloxypropyloxy)benzoyloxy]-2-methylbenzene (RM257) (**2**) and the E7 mixture (**3**), were bought from Synthon Chemicals GmbH & Co. KG. The photo-initiator phenyl-bis(2,4,6-trimethylbenzoyl)phosphine oxide

© 2024 The Author(s). Advanced Functional Materials published by Wiley-VCH GmbH

16163028, 2025, 3, Downloaded from https://advanced.onlinelibrary.wiley.com/doi/10.1002/adfm.202413513 by Universidad De Zaragoza, Wiley Online Library on [30/01/2025]. See the Terms and Conditions (https://onlinelibrary.wiley.com/terms-and-conditions) on Wiley Online Library for rules of use; OA articles are governed by the applicable Creative Commons License

(**4**) (TPO) was bought from Sigma–Aldrich. The radical inhibitor 2,6-di-tert-butyl-4-methylphenol (**5**) (BHT) and LC 4-cyano-4-pentylbiphenyl (**6**) (5CB) were ordered from TCI Deutschland GmbH. All the chemicals were used as received.

The LCG-ink 1 Contains Mesogens as Follows: **1**(32.8 wt.%), **2**(16.4 wt.%), **3**(49.2 wt.%) with the addition of the photoinitiator **4**(1.2 wt.%). The radical inhibitor, BHT, **5**(0.4 wt.%) was added to enhance the stability of the ink at higher temperatures. The chemicals were dissolved in dichloromethane. The mixture was then heated to 80 °C while mixing with a magnetic stirrer and while flowing nitrogen to evaporate the solvent. After removal of DCM, the remaining mixture was cooled to room temperature to obtain a transition to the nematic phase. To prepare LCG-ink 2, LCG-ink 1 was modified by adding an additional 20 wt.% of 5CB. The LCG-ink 2 used to fabricate LC gels therefore contains: RM 105 (27.33 wt.%), RM 257 (13.67 wt.%), E7 (41 wt.%), TPO (1 wt.%), BHT (0.33 wt.%), and 5CB (16.67 wt.%). After the preparation, the inks were filtered using a 0.45 um PTFE syringe filter (diameter 13 mm) to remove undissolved residues.

Developing the LCNs: After cross-linking the LC gel, the un-polymerized part of the ink was removed by keeping the LCG sample in isopropanol at 60° for 2–3 min. The un-polymerized mesogens dissolved in isopropanol. The samples were dried in air at ambient temperatures. After washing with a solvent and drying the 0.43 mg LCG sample resulted in 0.22 mg of a LCN. A negligible residue of the unpolymerized mixture remained in the LCN. The liquid crystalline networks were then observed in a polarization microscope.

Viscosity Measurements: Viscosity measurements were performed with a HR20 rheometer (TA Instruments) using a parallel plate geometry (upper plate had a diameter of 8 mm). The sample (100 µL) were placed between the plates and the gap was manually set to ≈1.2 mm to ensure appropriate sample loading. Measurements were performed at 25 °C at a shear rate range from 10 to 100 s^{-1}.

Preparing the Wedge Cell: The wedge cell was prepared using glass substrates with a thickness of 0.7 mm. The glass substrates induced homeotropic anchoring of the liquid crystal. The glass substrate was cut into pieces of ≈1.5 cm x 1 cm that were assembled with the help of spacers. At one end a spacer of 250 µm was used and at the opposite end a spacer with a thickness of 1 mm. A second substrate was then attached to the spacers to make a wedge cell. The wedge angle δ was measured by noting the exact separation of the spacers and the dimensions of the glass substrates. The LCG-ink was filled in this cell by capillary forces. (The Video S1 (Supporting Information) shows the schematics of the cell with a wedge angle δ.) The wedge angle δ differed slightly for each cell (between 7° and 9°) and was measured for each cell.

Magnetic Field and Magnetic Field Alignment of LCGs: Two permanent NdFeB magnets with a surface field of 0.3 T (as specified by the supplier) were positioned opposite each other with a spacing of 3.5 cm to obtain a magnetic field of 1300 Gauss in the center of the magnet pair. The magnets were inserted in a 3D-printed holder to ensure their parallel alignment and fixed separation. The magnetic field direction in-plane and also out-of-plane was set by rotating the holder (and hence the magnets). The 3D orientation of the magnetic field induced the corresponding director alignment (see Figure 8). The LC cell was placed at the center in between the two magnets. The alignment of the LCG-ink 2 in the field was observed in ≈1–2 min.

Photomask: The photomask of the desired shape was cut from aluminum foil. The photomask was placed on top of the cell at a desired position to select the LC volume for cross-linking. Photopolymerization of the LCG-ink was obtained after exposure of 365 nm light from a UV lamp (UV consulting) directed through a lens to the sample with an intensity of 1 W cm^{-2} at the sample for 1 to 2 min through the photomask. The mask was physically moved to a new position and the process was repeated to fabricate the cross-linked LC gel shown in Figure 2. Voxel boundaries could be clearly discerned with a polarization optical microscope (Leica DM 27 100 P).

Supporting Information

Supporting Information is available from the Wiley Online Library or from the author.

Acknowledgements

The authors thank Prof. Dr. Eva Blasco for providing samples as well as helpful discussions, Dr. Alexander Song for his assistance in developing the optics setup, and Dr. Dimitris Missirlis for his assistance with rheological measurements. The described research is part of the project STORM-BOTS. This project has received funding from the European Union's Horizon 2020 research and innovation program under Grant Agreement No 956150. Funding has also been received by Grant PID2020-118485RB-I00 funded by MCIN/AEI/10.13039/ 501100011033, and by CIBER-Consorcio Centro de Investigacioń Biomedíca en Red (CB16/01/00263), Instituto de Salud Carlos III (Spanish Ministry of Science and Innovation and European Commission, European Regional Development Fund). This work has been supported by Gobierno de Aragón, FEDER (EU) and Fondo Social Europeo (DGA E15_20R).

Open access funding enabled and organized by Projekt DEAL.

Conflict of Interest

The authors declare no conflict of interest.

Data Availability Statement

The data that support the findings of this study are available in the supplementary material of this article.

Keywords

birefringence, liquid crystalline materials, low magnetic field, polarization, wedge cell, 3D director

Received: July 26, 2024
Revised: September 23, 2024
Published online: September 24, 2024

[1] T. J. White, D. J. Broer, *Nat. Mater.* **2015**, *14*, 1087.
[2] M. Warner, *Annu. Rev. Condens. Matter Phys.* **2020**, *11*, 125.
[3] D. J. Broer, G. N. Mol, *Polym. Eng. Sci.* **1991**, *31*, 625.
[4] R. S. Kularatne, H. Kim, J. M. Boothby, T. H. Ware, *J. Polym. Sci., Part B: Polym. Phys.* **2017**, *55*, 395.
[5] D. Liu, D. J. Broer, *Langmuir* **2014**, *30*, 13499.
[6] H. K. Bisoyi, Q. Li, *Chem. Rev.* **2016**, *116*, 15089.
[7] D. J. Broer, *Adv. Mater.* **2020**, *32*, 1905144.
[8] O. M. Wani, H. Zeng, A. Priimagi, *Nat. Commun.* **2017**, *8*, 15546.
[9] A. Kotikian, C. McMahan, E. C. Davidson, J. M. Muhammad, R. D. Weeks, C. Daraio, J. A. Lewis, *Sci. Rob.* **2019**, *4*, eaax7044.
[10] E. R. Espíndola-Pérez, J. Campo, C. Sánchez-Somolinos, *ACS Appl. Mater. Interfaces* **2023**, *16*, 2704.
[11] S. Palagi, A. G. Mark, S. Y. Reigh, K. Melde, T. Qiu, H. Zeng, C. Parmeggiani, D. Martella, A. Sanchez-Castillo, N. Kapernaum, *Nat. Mater.* **2016**, *15*, 647.
[12] K. M. Herbert, H. E. Fowler, J. M. McCracken, K. R. Schlafmann, J. A. Koch, T. J. White, *Nat. Rev. Mater.* **2022**, *7*, 23.
[13] D. J. Broer, *Mol. Cryst. Liq. Cryst.* **1995**, *261*, 513.
[14] J. J. Wie, K. M. Lee, T. H. Ware, T. J. White, *Macromolecules* **2015**, *48*, 1087.

© 2024 The Author(s). Advanced Functional Materials published by Wiley-VCH GmbH

16163028, 2025, 3, Downloaded from https://advanced.onlinelibrary.wiley.com/doi/10.1002/adfm.202413513 by Universidad De Zaragoza, Wiley Online Library on [30/01/2025]. See the Terms and Conditions (https://onlinelibrary.wiley.com/terms-and-conditions) on Wiley Online Library for rules of use; OA articles are governed by the applicable Creative Commons License

[15] A. H. Gelebart, D. J Mulder, M. Varga, A. Konya, G. Vantomme, E. Meijer, R. L. Selinger, D. J. Broer, *Nature* **2017**, *546*, 632.
[16] Y. Xia, G. Cedillo-Servin, R. D. Kamien, S. Yang, *Adv. Mater.* **2016**, *28*, 9637.
[17] H. Zeng, P. Wasylczyk, G. Cerretti, D. Martella, C. Parmeggiani, D. S. Wiersma, *Appl. Phys. Lett.* **2015**, *106*, 11.
[18] T. H. Ware, J. S. Biggins, A. F. Shick, M. Warner, T. J. White, *Nat. Commun.* **2016**, *7*, 10781.
[19] L. T. de Haan, C. Sánchez-Somolinos, C. M. Bastiaansen, A. P. Schenning, D. J. Broer, *Angew. Chem., Int. Ed.* **2012**, *51*, 12469.
[20] M. E. McConney, A. Martinez, V. P. Tondiglia, K. M. Lee, D. Langley, I. I. Smalyukh, T. J. White, *Adv. Mater.* **2013**, *25*, 5880.
[21] H. Zeng, O. M. Wani, P. Wasylczyk, R. Kaczmarek, A. Priimagi, *Adv. Mater.* **2017**, *29*, 1701814.
[22] T. H. Ware, M. E. McConney, J. J. Wie, V. P. Tondiglia, T. J. White, *Science* **2015**, *347*, 982.
[23] L. T. de Haan, V. Gimenez-Pinto, A. Konya, T. S. Nguyen, J. M. Verjans, C. Sánchez-Somolinos, J. V. Selinger, R. L. Selinger, D. J. Broer, A. P. Schenning, *Adv. Funct. Mater.* **2014**, *24*, 1251.
[24] S. Li, G. Librandi, Y. Yao, A. J. Richard, A. Schneider-Yamamura, J. Aizenberg, K. Bertoldi, *Adv. Mater.* **2021**, *33*, 2105024.
[25] L. Ceamanos, Z. Kahveci, M. López-Valdeolivas, D. Liu, D. J. Broer, C. Sánchez-Somolinos, *ACS Appl. Mater. Interfaces* **2020**, *12*, 44195.
[26] C. P. Ambulo, J. J. Burroughs, J. M. Boothby, H. Kim, M. R. Shankar, T. H. Ware, *ACS Appl. Mater. Interfaces* **2017**, *9*, 37332.
[27] M. López-Valdeolivas, D. Liu, D. J. Broer, C. Sánchez-Somolinos, *Macromol. Rapid Commun.* **2018**, *39*, 1700710.
[28] A. Kotikian, R. L. Truby, J. W. Boley, T. J. White, J. A. Lewis, *Adv. Mater.* **2018**, *30*, 1706164.
[29] J. Zhao, L. Zhang, J. Hu, *Adv. Intell. Syst.* **2022**, *4*, 2100065.
[30] A. Münchinger, V. Hahn, D. Beutel, S. Woska, J. Monti, C. Rockstuhl, E. Blasco, M. Wegener, *Adv. Mater. Technol.* **2022**, *7*, 2100944.
[31] A. Münchinger, L. Y. Hsu, F. Fürniß, E. Blasco, M. Wegener, *Mater. Today* **2022**, *59*, 9.
[32] P. G. De Gennes, J. Prost, *The Physics of Liquid Crystals*, Oxford University Press, Oxford **1993**.
[33] M. Tabrizi, T. H. Ware, M. R. Shankar, *ACS Appl. Mater. Interfaces* **2019**, *11*, 28236.
[34] Y. Yao, J. T. Waters, A. V. Shneidman, J. Cui, X. Wang, N. K. Mandsberg, S. Li, A. C. Balazs, J. Aizenberg, *Proc. Natl. Acad. Sci. U.S.A.* **2018**, *115*, 12950.
[35] B. Ni, G. Liu, M. Zhang, P. Keller, M. Tatoulian, M. H. Li, *CCS Chem.* **2022**, *4*, 847.
[36] S. Li, M. Aizenberg, M. M. Lerch, J. Aizenberg, *Acc. Mater. Res.* **2023**, *4*, 1008.
[37] L. M. Blinov, *Sci. Prog.* **1986**, *70*, 263.
[38] F. Ania, A. Flores, H. Kricheldorf, F. J. Baltá-Calleja, *Polymer* **2003**, *44*, 5909.
[39] B. Ni, G. Liu, M. Zhang, M. Tatoulian, P. Keller, M. H. Li, *ACS Appl. Mater. Interfaces* **2021**, *13*, 54439.
[40] Y. Wang, J. An, H. Kim, S. Jeong, H. Kim, J. Park, S. Ko, J. Son, H. Lee, arXiv:2401.06590v1.
[41] B. Frisken, J. Carolan, P. Palffy-Muhoray, J. Perenboom, G. Bates, *Mol. Cryst. Liq. Cryst.* **1986**, *3*, 57.
[42] T. Kosa, P. Palffy-Muhoray, *Liq. Cryst. Today* **1996**, *6*, 7.
[43] A. Diogo, A. Martins, *J. Phys.* **1982**, *43*, 779.
[44] J. Shin, M. Kang, T. Tsai, C. Leal, P. V. Braun, D. G. Cahill, *ACS Macro Lett.* **2016**, *5*, 955.
[45] A. Buka, W. De Jeu, *J. Phys.* **1982**, *43*, 361.
[46] H. G. Hauck, G. Heppke, Flüssigkristalle. In "Lehrbuch der Experimentalphysik" (ed. Bergmann-Schaefer) **2008**, vol. *5*, 649–710.
[47] I. Muševič, *Liquid crystal colloids*, Springer, New York City **2017**.
[48] M. L. Magnuson, B. Fung, *J. Chem. Phys.* **1994**, *100*, 1470.
[49] H. Shahsavan, A. Aghakhani, H. Zeng, Y. Guo, Z. S. Davidson, A. Priimagi, M. Sitti, *Proc. Natl. Acad. Sci. USA* **2020**, *117*, 5125.
[50] R. Oldenbourg, *Nature* **1996**, *381*, 811.
[51] J. F. Wu, Y. T. Zhang, *Optik-International Journal for Light and Electron Optics.* **2013**, *124*, 2667.
[52] M. Avendaño-Alejo, *Opt. Express* **2005**, *13*, 2549.
[53] J. Pavlin, N. Vaupotič, M. Čepič, *Eur. J. Phys.* **2013**, *34*, 331.
[54] K. Kowiorski, J. Kędzierski, Z. Raszewski, M. Kojdecki, J. Herman, E. Miszczyk, W. Piecek, *Acta Phys. Pol. A* **2013**, *124*, 946.
[55] J. Kędzierski, Z. Raszewski, M. Kojdecki, E. Kruszelnicki-Nowinowski, P. Perkowski, W. Piecek, E. Miszczyk, J. Zieliński, P. Morawiak, K. Ogrodnik, *Opto-Electronics Review* **2010**, *18*, 214.
[56] E. Hecht, Optics, 4e, Addison & Wesley, New York **2002**.
[57] M. Pfeifer, P. Fischer, *Opt. Express* **2011**, *19*, 16508.
[58] A. Ghosh, W. Hill, P. Fischer, *Phys. Rev. A* **2007**, *76*, 055402.

© 2024 The Author(s). Advanced Functional Materials published by Wiley-VCH GmbH

16163028, 2025, 3, Downloaded from https://advanced.onlinelibrary.wiley.com/doi/10.1002/adfm.202413513 by Universidad De Zaragoza, Wiley Online Library on [30/01/2025]. See the Terms and Conditions (https://onlinelibrary.wiley.com/terms-and-conditions) on Wiley Online Library for rules of use; OA articles are governed by the applicable Creative Commons License